Species-Specific Sputtering Measurements with Cavity Ring-Down Spectroscopy

V.K. Surla[*], L. Tao[†], A.P. Yalin[‡]
Colorado State University, Fort Collins, CO, 80523

We report sputtering studies using cavity ring-down spectroscopy (CRDS). The high sensitivity of the technique and its non-intrusive nature make it amenable to both in situ device studies as well as basic characterization studies. We provide demonstrative measurements of sputtered particles showing the ability to determine species-specific number density and velocity. We summarize a spatial-scanning approach for differential sputter yield measurements and give a measurement example based on a tantalum target. We discuss the use of CRDS for measurement of multi-component materials and provide experimental results for detection of a Fe-Mn target as well as a proposed detection scheme for boron nitride.

Nomenclature

c	=	speed of light
g_i	=	degeneracy of level i
k	=	absorption coefficient
k_{Eff}	=	effective absorption coefficient
l	=	cavity length
y	=	differential sputter yield
A_{ki}	=	Einstein A coefficient
Abs_{Eff}	=	effective absorbance
J	=	total angular momentum quantum number
M_i	=	molar mass of species i
R	=	mirror reflectivity
S	=	ring-down signal
Y	=	total sputter yield
Y_b	=	target displacement (in spatial scans)
α	=	polar angle (relative to target normal)
β	=	ion incidence angle (relative to target normal)
λ	=	wavelength
ν	=	frequency
ϕ	=	azimuthal angle (in plane of target surface)
ρ	=	density of target material
τ	=	ring-down time

I. Introduction

The lifetimes of state-of-the-art electric propulsion ion and plasma thrusters are largely limited by sputter erosion of grids and other components. Sputtering may also lead to unwanted deposits that can lead to surface contamination and associated problems. Sputtering is normally characterized by the total sputter yield, Y, i.e. the number of atoms ejected per incident ion. While total sputter yields are generally sufficient for determination and

[*] Graduate Research Associate, Mechanical Engineering, Colorado State University (now with Department of Chemistry, Stanford University)
[†] Graduate Research Associate, Mechanical Engineering, Colorado State University
[‡] Assistant Professor, Mechanical Engineering, Colorado State University, AIAA Member.

modeling of erosion rates and lifetimes, they do not provide the needed angular information for computation of trajectories for redeposition and contamination studies. In such cases differential sputter yields, $y(\alpha,\phi)$, i.e. the number of atoms ejected per incident ion per ejection solid angle, are required. The situation is increasingly complex when the materials of interest are multicomponent materials as are often used for insulators and thermal control surfaces (e.g. boron nitride, quartz, inconel etc.) In such cases, a full characterization of the sputtering requires species-specific differential sputter yields, i.e. $y_i(\alpha,\phi)$, for each component i of the material of interest. Modeling of sputtering of multicomponent materials shows that different constituents typically sputter differently not only in amplitude but also in their angular profiles[1]. Knowledge of the species-specific sputtering is of particular importance in such studies owing to the different sticking coefficients and deleterious effects of the different species.

Several techniques are available for measurements of total and differential sputter yields. For example, total and differential sputter yield profiles have been measured with weight loss[2], collector plates[3-4], quartz crystal microbalance[5-11], and radioactive tracers[12]. Generally the aforementioned techniques are not species-specific while techniques such as mass spectrometry[13] and Rutherford backscattering[14-15] do allow species-specific measurements. Additionally, optical techniques such as optical emission spectroscopy[16-17], laser induced fluorescence[18-20], and multi-photon ionization coupled to a time of flight mass spectrometer[21-23] have been used for (species-specific) sputtering measurements. The use of LIF has been particularly extensive, and has proven to be very effective for velocity measurement though challenging for quantitative number density.

The work presented here builds upon our previous development of cavity ring-down spectroscopy (CRDS) for sputtering measurements[24-27]. CRDS is a highly sensitive laser-based absorption method allowing species-specific measurement of concentrations of trace species. The technique is used extensively for trace-species measurement in flames, plasmas, and the atmosphere and we have developed its use for the study of sputtered particles in EP applications. Essentially, the absorbing sample, i.e. plume of sputtered particles, is housed within a high-finesse optical cavity formed between highly reflective mirrors. The use of the optical cavity greatly increases the (effective) absorption path length and therefore the measurement sensitivity. We have previously demonstrated measurements of number density and velocity of sputtered particles, from which we can determine total sputter yields. We have also demonstrated the use of a spatial scanning approach to infer differential sputter yields[26-27], and the ability to make measurements of multi-component materials[26]. The high sensitivity and non-intrusive nature of CRDS make it amenable to in situ device studies, e.g. real time monitoring of thruster erosion by measurement of sputtered particles in the plume. In comparison to LIF, we view that CRDS is better suited to obtain quantitative measurements of number density since signal analysis is simpler, though LIF remains attractive for measuring velocity profiles. As with other laser techniques, the main practical impediment in applying CRDS is the need to study optically accessible species, i.e. to work at wavelengths where optical sources, detectors, and high-reflectivity mirrors are available. In terms of signal analysis, the path-integrated nature of CRDS can be challenging and requires the use of inversion (tomographic) techniques to recover spatially resolved profiles, as we do in our differential sputter yield measurements.

In this contribution we recap the CRDS approach and provide novel measurements demonstrating the ability to infer angular information for differential sputter yields and to study multicomponent materials. In Section II we summarize the CRDS technique, while Section III describes the base setup used for experimental measurements. Differential sputter yield measurements of tantalum are presented in Section IV and are compared with past quartz crystal microbalance (QCM) measurements. Measurements of multi-component materials are presented in Section V including a study of an Fe:Mn target and a proposed detection scheme for boron nitride. Conclusions are provided in Section VI.

II. Cavity Ring-Down Spectroscopy

Cavity ring-down spectroscopy is a highly sensitive laser-based absorption method allowing measurement of concentrations of trace species. Detailed reviews of the technique may be found in references 28 and 29. Our previous development of CRDS for sputter diagnostics has been previously described[24-27]. As shown in Fig.1, the absorbing sample is contained within a high-finesse optical cavity typically formed from two (or three) high-reflectivity (R) mirrors with R ~0.9999. As the laser beam is coupled into the cavity, the light bounces back-and-forth many times within the cavity. Upon each reflection at the rear cavity-mirror, a small fraction of the cavity light leaks out to a photodetector that measures the decay of light intensity within the optical cavity. The decay is characterized by the 1/e time of decay termed the ring-down time, τ. The light decays primarily due to mirror reflective loss when there is no absorber present, and decays faster when resonant with sample absorption. The

change in ring-down times can be related to the sample's absorbance (concentration). The technique provides high sensitivity owing to a combination of long effective path length and insensitivity to laser energy fluctuations.

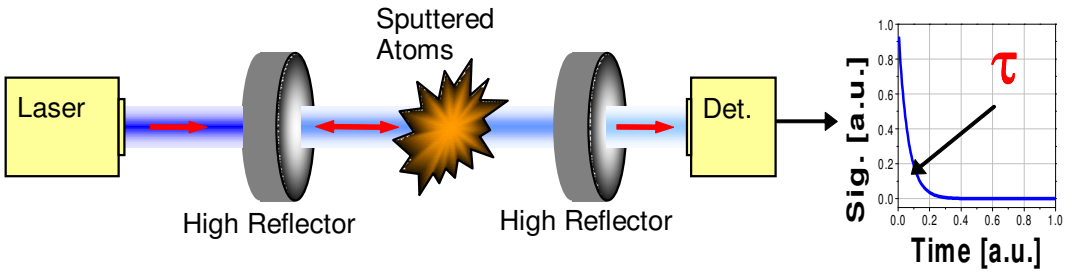

Figure 1. Schematic diagram of CRDS setup.

Under appropriate conditions, the ring-down signal $S(t,\nu)$ decays (single-) exponentially versus time as[30-31]:

$$S(t,\nu) = S_0 \exp\left[-t/\tau(\nu)\right]$$

$$1/\tau(\nu) = \frac{c}{l}\left[\int k_{Eff}(x,\nu)dX + (1-R)\right] \quad ; \quad k_{Eff}(\nu) \equiv \int_{-\infty}^{+\infty} d\nu'\, L(\nu'-\nu)\, k(\nu') \tag{1}$$

where τ is the 1/e time of the decay (termed the ring-down time), c is the speed of light, l is the cavity length, $k_{eff}(\nu)$ is the effective absorption coefficient, X is the spatial coordinate along the optical axis, ν is the laser frequency, $1\text{-}R$ is the effective mirror loss (including scattering and all cavity losses), and $L(\nu)$ is the laser lineshape function. As in conventional absorption, the effective absorption coefficient accounts for line broadening arising from the laser lineshape. In practice, the measured ring-down signal is fitted with an exponential, and the ring-down time τ is extracted. Combining τ with the "empty cavity ring-down time", τ_0 (which in practice is measured by detuning the laser) allows determination of the (effective) sample absorbance, Abs_{Eff}, and the path-integrated (effective) absorption coefficient, k_{Eff}:

$$Abs_{Eff}(\nu) \equiv \int k_{Eff}(\nu)\, dX = \frac{l}{c}\left[\frac{1}{\tau(\nu)} - \frac{1}{\tau_0}\right] \tag{2}$$

As in conventional absorption, both the laser and absorber lineshapes are needed to determine the actual absorbance (and number density) if the effective absorbance is measured at a single wavelength. A more practical approach is to scan the laser frequency across the absorption line and to measure the frequency-integrated spectrum (i.e. the line area). Because the area of the effective absorbance spectrum is equivalent to the area of the (actual) absorbance spectrum, this method removes lineshape dependences. Assuming the absorption line parameters are known, the measured area $\int Abs_{Eff}(\nu)d\nu$ of a transition from lower state i to upper state k can be readily converted to the path-integrated concentration of the lower state n_i as:

$$\int n_i dX = 8\pi \frac{g_i}{g_k} \frac{\nu_{ki}^2}{A_{ki} c^2} \left(\int Abs_{Eff}(\nu)\, d\nu \right) \tag{3}$$

where g_i, g_k are the level degeneracies, ν_{ki} is the transition frequency, and A_{ki} is the transition Einstein A coefficient. As reported in our earlier work, for the species and conditions of interest, the measured lower state population can be converted to overall species population through the energy level distributions[25]. We use equation (3) to determine the path-integrated concentration along a chord. For differential sputter yield measurements we obtain path-integrated values along a series of chords and then use modeling to infer angular profiles (see Section IV).

III. Experimental

A. Basic Setup

The experimental setup used in the current work is shown in Figure 2. Our past work[25-27] reports most details of the apparatus so here we only summarize the key aspects. A broadly tunable optical parametric oscillator (OPO) laser system (doubled idler) is used as the light source to probe the required optical transitions which are generally in the 370-405 nm region. The optical cavity is formed using a pair of high-reflectivity mirrors (R≈0.9998) and is integrated with the chamber in such a way that the sputtered particles are roughly equidistant between the mirrors. The ring-down signals are collected behind the output mirror with a fast photomultiplier tube (Hamamatsu R3896) and passed to a custom data acquisition code which fits the signals with exponentials to extract the ring-down (1/e) times. A given measurement requires recording of the absorbance spectrum and is achieved by scanning the laser across the given absorption feature(s) and determining the ring-down time at each laser wavelength step.

The ring-down cavity is integrated with a sputtering facility consisting of an ion beam and sputtering target within a vacuum chamber. A roughing and turbo-pump (Turbo-V550) are used to bring the pressure to approximately 10^{-6}-10^{-7} torr under no-flow conditions. With the ion beam operating, the chamber pressure is ~10^{-5} torr. At these conditions, the sputtered atoms are in a collisionless free-molecular regime (Knudsen number << 1). A small argon flow (1 sccm) is fed to the system and the ion beam is extracted from an 8-cm diameter structurally integrated thruster using an IonTech power supply (MPS 3000). The ion beam is (approximately) normally incident on the target. The ion source is modified to operate with refractory metal filaments instead of hollow cathodes present in the initial design for both cathode and neutralizer cathodes. For the experiments presented here the ion beam generally has an 8 cm diameter. A characterization of the ion beam was conducted using a (3-D translating) button probe to measure the current density profile. Total beam currents are generally ~30 mA with current densities of approximately 0.5 mA/cm^2 [27]. We have verified that our measurements are unaffected by poisoning.

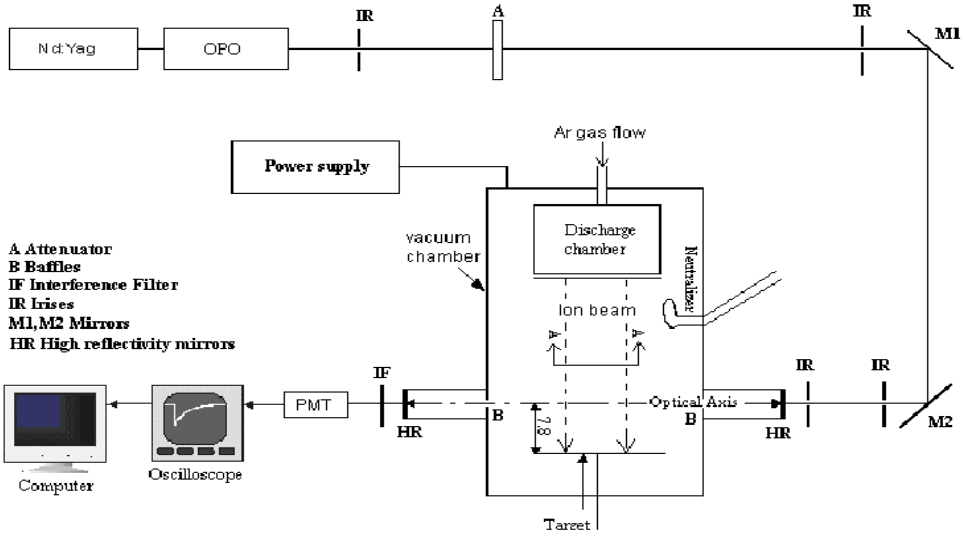

Figure 2. Schematic diagram of CRDS set-up. An ion source and target are housed within a vacuum chamber. Sputtered species are created as the ion beam bombards the target. The plume of the sputtered species is intersected by the optical axis of the high-finesse ring-down cavity. An OPO laser system is used as the light source, and a photomultiplier tube (PMT) detects the light exiting the cavity.

For differential sputter yields we require spatial measurements, i.e. measurements along different chords through the plume of sputtered particles. For this purpose we use two translational stages for movement of the sputtering target with a precision of ~1 mm. This is conceptually similar to moving our optical axis relative to the target, but movement of the target is considerably simpler and does not affect cavity alignment. One stage moves the target in the *Z*-direction towards or away from the ion source (and optical axis), while the second moves the target in the *Y*-

direction (see Figure 3), which is the direction perpendicular to both the optical axis and the ion beam direction. We use Y_b to denote a given positioning of target (with Y_b=0 corresponding to the target being centered with respect to the optical axis). At a fixed Z position, we measure the CRDS signal at a series of Y positions, thereby obtaining spatial profiles. Note that the X-Y-Z coordinate system is fixed relative to the optical axis (and ion beam), but not relative to the target.

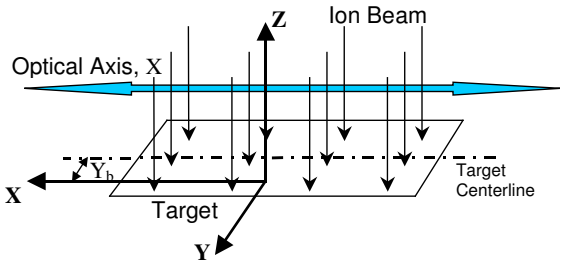

Figure 3. Coordinate system.

B. Characteristic Spectra

Figure 4 shows an example of a CRDS measurement of sputtered iron including four absorption lines[25]. The conditions for the argon ion beam are a current of 20 mA and beam voltage of 750 V. In the figure, the symbols are experimental measurements while the solid line is a series (sum) of Voigt profiles fitted to the peaks (with a single Voigt used for each absorption feature). The measured lines in the absorbance spectrum originate from the three lowest energy levels (J=4,3,2) of the split ground state (^{5}D multiplet), and the fitted Voigt areas of the absorption lines can be used to determine the (path-integrated) number densities of these levels[25]. In this case our characterization of excitation temperature suggests that >93% of the overall iron population is in these measured states (and greater than 99% of the iron is in the ground state multiplet)[25]. Therefore, we can scale the (sum of the) population of the 3 measured states to infer the overall iron population with relatively high fidelity. In this way we find a path-integrated number density of iron atoms of $2.3\pm0.2\text{x}10^{10}$ cm^{-2}. The uncertainty is due to uncertainty in the Voigt fitted areas, population fractions, and Einstein A coefficients. The path-integrated concentration value is in good agreement with modeled results based on a finite element model of the target and optical-axis.

The spectral lineshapes of the measured features are due to Doppler shift contributions based on the particle angular spread and velocity distribution. We have demonstrated measurements of the velocity distribution from the spectral lineshapes[26].

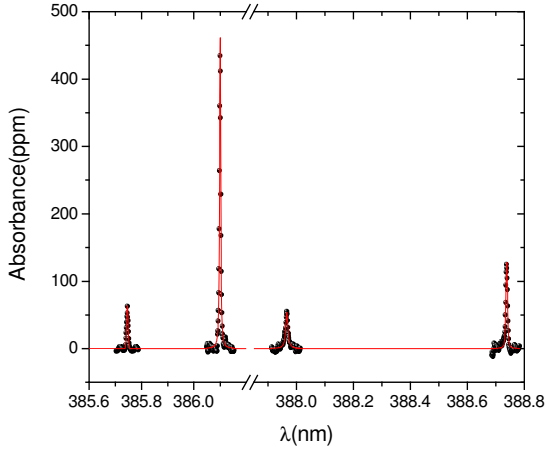

Figure 4. Absorbance spectrum of sputtered iron measured by CRDS.

IV. Differential Sputter Yield Measurements

We have reported differential sputter yield measurements in our earlier work[26-27]. In summary, the approach relies upon scanning a thin "strip" of target material laterally relative to the (fixed) optical axis, i.e. changing the target displacement Y_b. At each lateral position, Y_b, the CRDS detection system measures the path-integrated number density of sputtered particles along the optical axis, X. We term the dependence of CRDS signal (path-integrated number density) on the lateral position, Y_b, as the Spatial Profile. In the analysis, we employ a numerical model to infer the differential sputter yield from the spatial profile. The approach is shown schematically in Figure 5.

The numerical model for simulation of the path-integrated concentration values (i.e. the Spatial Profile) employs a finite element scheme for the target and optical axis, the experimentally measured current density profile of the ion beam, and the differential sputter yield profile[26-27]. The approach is to simulate spatial profiles for a range of differential sputter yield profiles, and then seek the best agreement with the measured CRDS spatial profile. In principle, different mathematical forms of the differential sputter yield could be assumed (e.g. the Modified Zhang profiles that we employ in quartz crystal microbalance measurements[8-9]) though in this work we assume a functional form:

$$y(\alpha) = \frac{Y}{\pi}\cos(\alpha)\left(1 + a\left(1 - 2\cos^2(\alpha)\right)\right) \tag{4}$$

where Y is the total sputter yield, α is the polar angle above the target (measured relative to the surface normal), and the parameter 'a' allows a range of profile shapes between under-cosine (a>0) and over-cosine (a <0)[32]. Figure 6 shows polar plots of examples of differential sputter yield profiles from equation (4).

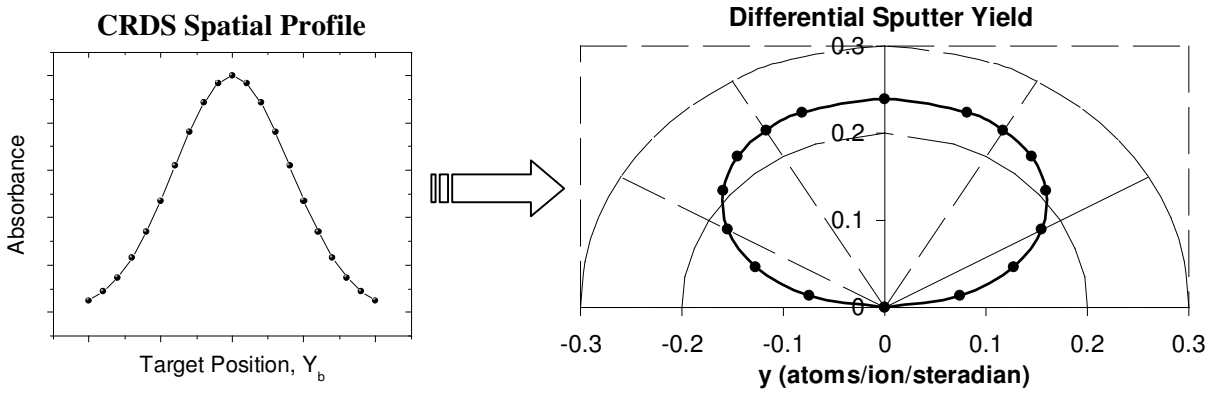

Figure 5. Measurement approach for determination of differential sputter yield.

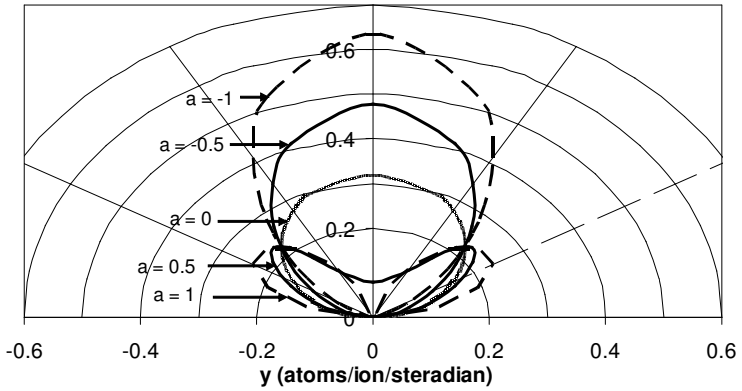

Figure 6. Differential sputter yield profiles for different values of parameter *a*.

Our past work has demonstrated the measurement approach for molybdenum and here we present results for sputtering of tantalum. CRDS measurements of Tantalum (Ta) due to argon ion bombardment are obtained in the diagnostic test-bed described earlier. The CRDS scheme for detection of Ta is based on probing a ground state absorption line at 391.963 nm vacuum (391.852 nm air). The ground state has no fine structure so the single line measurement allows determination of the (ground state) number density. An 8 cm x 4 cm tantalum target is used. The distance between the optical axis and the target (Z) is fixed at 2 cm. The left of Figure 7 (symbols) shows the CRDS spatial profile for 750 eV argon ions incident on the Ta target at a height of optical axis above target of Z=2 cm. Using the sputtering model, the profile that best fits the measured spatial profile is found to be $a = 0.0 \pm 0.1$ (error bar based on repeatability), corresponding to a diffuse (cosine) differential sputter yield profile. This fitted profile is shown as a solid black line in the polar plots at right of Figure 7. For validation, the CRDS differential sputter yield result is compared with QCM measurements reported for Ar^+ ion on Ta[7]. The QCM profile is shown in the polar plot as a brown line, while a diffuse (cosine) profile is also shown for comparison. Because in this case the CRDS measurement also yields a diffuse result, the CRDS and diffuse plots should be coincident (and the slight mismatch is owing to the normalizations). Note that the asymmetric form of the QCM polar plot is owing to measurement error and therefore we can not expect exact match between the CRDS and QCM. Nonetheless, the close agreement between the CRDS and QCM measurements of differential sputter yield are viewed as validation of

the CRDS measurement. Possible shortcomings of the CRDS modeling approach include the assumption of angularly-independent ejection velocity, and the assumed (single parameter) form of the differential sputter yield.

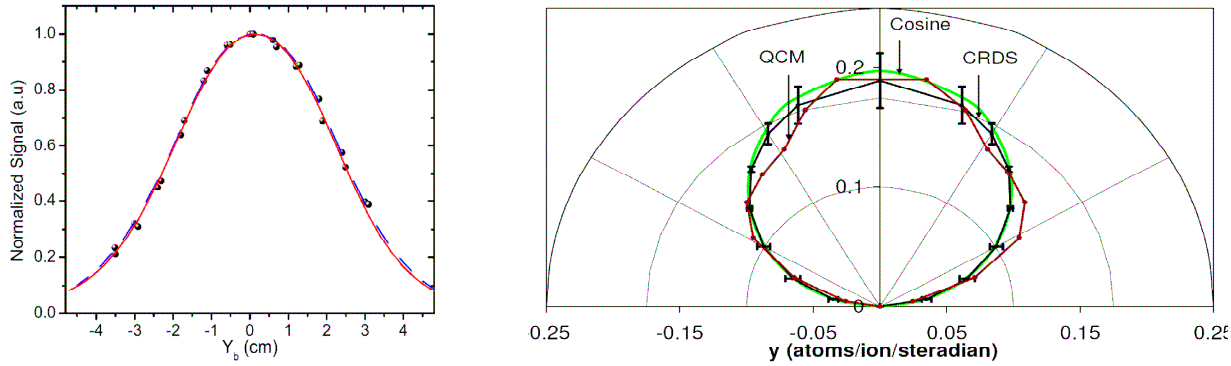

Figure 7. Differential sputter yield measurement of sputtered tantalum. Left: CRDS spatial profile. Symbols – CRDS data, Red solid line – model fit to CRDS data (a=0.0), Blue dashed line – modeled profile based on QCM data. Right: Polar plot of differential sputter yield profiles. Black line – modeled profile from fit to CRDS data (a=0.0), Brown line – QCM data, Green line – diffuse profile (see text).

V. Multi-Component Material Measurements

Sputter yields for many single-component materials are well known (at least for energies well above the threshold); however, the sputter yields for multi-component materials are in many cases not known. Further, owing to the relative complexity of these materials and the sputtering processes, it is generally difficult to theoretically or numerically[1] predict their sputtering properties. As discussed in the introduction, the majority of existing (non-optical) techniques do not give species-specific information though techniques such as QCM measurements and weight loss still may be used for sputtering studies. CRDS can be used for species-specific sputter measurements and more generally is attractive owing to its high sensitivity and in situ capabilities. In our past work we have demonstrated CRDS measurements of inconel (detection of iron, chromium, and molybdenum)[26]. Here we show results of sputtering from a Fe:Mn target and present the detection scheme for future boron nitride measurements.

A. Iron-Manganese

In this section, initial CRDS measurements of Fe-Mn target are presented. The constituents of Fe-Mn (by atomic percentage) as specified by the supplier are: Fe 50 %, Mn 50%. Both components are optically accessible by CRDS. Detection of Fe is as described in Section III. The CRDS detection of Mn from is based on probing the absorption line of Mn in the electronic ground state $3d^5\ 4s^2$ at 403.42 nm vacuum (403.31 nm air). Manganese has no fine structure in its ground state and the next lowest energy level is 17052.29 cm^{-1}, so that to a good approximation all population is in the measured ground state energy level.

The experimental conditions are a 750 eV Ar+ beam striking an Fe-Mn target of 8 cm (in the beam direction) by 4 cm, with the optical axis at a height Z=2 cm above the target. Prior to measurements, the target was sputter cleaned by Ar+ ions of energy 750 eV for more than 30 minutes. Figure 8 shows absorbance spectra of iron and manganese from the sputtered Fe-Mn target. The path integrated concentration and velocity of the species are obtained from the measured CRDS lineshapes. At the optical axis centerline, the resulting path-integrated concentration of Fe and Mn are $1.9\pm0.2\text{x}10^{10}$ cm^{-2} and $1.4\pm0.1\text{x}10^{10}$ respectively. At steady state the relative composition (ratio) of fluxes of sputtered particles should mimic the composition ratio of constituents in the target, which is approximately the case here. Precise determination of the flux requires full knowledge of velocity profiles and angular sputtering profiles and has not been addressed.

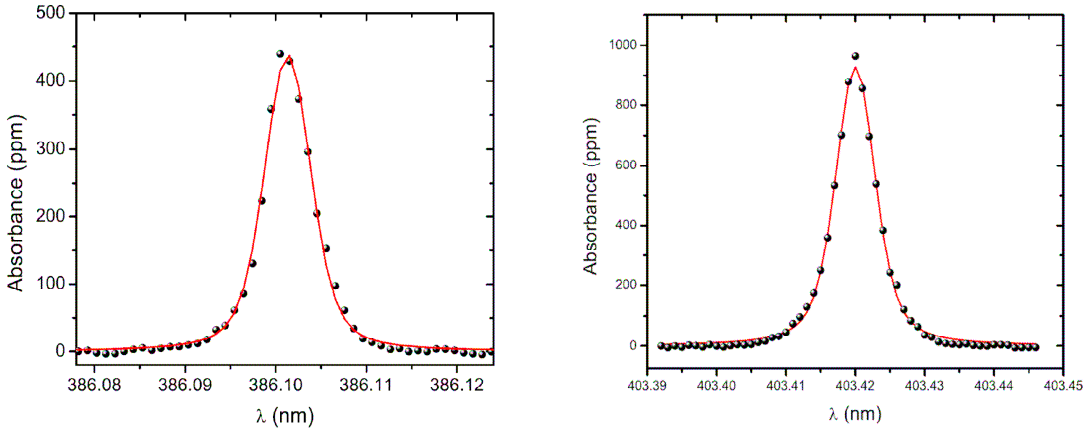

Figure 8. CRDS absorbance spectra of iron (left) and manganese (right) from sputtered Fe:Mn target.

B. Boron Nitride

From the point of view of Hall thruster erosion (and contamination) the sputtering of boron nitride (BN) is of primary importance owing to its widespread used as an insulator material in acceleration channels. However, there is a lack of available sputtering data on BN and a lack of available measurement techniques for *in situ* thruster studies. Here, we consider the use of CRDS to study boron nitride. The approach is to detect sputtered boron atoms in the vicinity of 250 nm (ultraviolet). (For initial consideration, assume that BN sputters primarily as atoms of boron, and atoms of nitrogen.) CRDS measurements of boron present challenges owing to reduced mirror reflectivity and reduced number densities (low sputter yields). Mirror reflectivity in the ultraviolet tends to be low (R~0.995-0.998) as compared to near-UV or visible (R>~0.9999) owing to challenges of the optical coatings and their absorption. In order to achieve the required detection sensitivity with lower reflectivity mirrors we will implement cw-CRDS, i.e. CRDS employing continuous-wave lasers as opposed to pulsed lasers. As a first step toward the cw-CRDS system we aim to perform (lower sensitivity) measurements of BN using pulsed-CRDS at high number density conditions.

Figure 9 shows a simulated absorbance spectrum for anticipated conditions in the sputter chamber of our CRDS test-bed. Conditions are selected to enable elevated boron concentrations to facilitate initial demonstrative measurements using pulsed-CRDS. Subsequent thruster measurements with our cw-CRDS system will be at several orders of magnitude lower concentration. The spectrum of Figure 9 is computed using Beer's Law and assumes a total sputter yield = 0.3 (for ~keV ions), beam current = 30 mA, height above target =1 cm, and path integrated boron concentration (based on these parameters) of 5×10^{10} cm^{-2}. The anticipated detection limit for pulsed-CRDS with commercially available mirrors is about 50 ppm (for this spectral region).

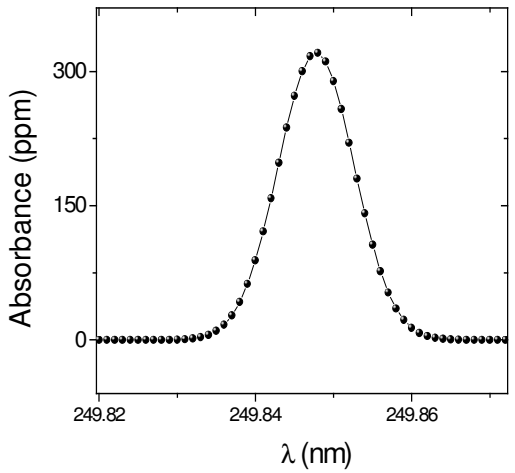

Figure 9. Simulated absorbance spectrum for boron.

VI. Conclusions

Sputter erosion plays a significant role in EP owing to the life limitations it imposes and associated contamination effects. Sputter measurements are required for both basic material characterizations (to provide inputs to numerical models) and for real-time device testing. Although several optical and non-optical measurement

techniques exist, there is a dearth of techniques that are capable of sensitive quantitative measurements (especially species- and state-specific measurements) while being amenable to in situ applications. Owing to the shortcomings of existing methods, we have been focused on development of CRDS as a sputter gauge.

In this work, we have summarized the CRDS measurement technique and the setup of our diagnostic test-bed. In addition to (line of sight) number density and velocity measurements we employ a spatial scanning and inversion technique to measure differential sputter yields, i.e. the angular profiles of sputtered particles. We have demonstrated the spatial scanning approach for sputtering of tantalum by argon ions and we find a nearly diffuse (cosine) differential sputter yield profile that is in good agreement with past measurements from a quartz crystal microbalance. We also consider the sputtering of multi-component targets. We have provided sputter measurements of an iron-manganese target in which both species are detected. These measurements are in reasonable agreement with expectations based on the target composition. Finally, we discuss proposed measurements of boron nitride, a material of high relevance to Hall thrusters. The measurement scheme is based on detection of boron in the ultra-violet.

Acknowledgments

The authors would like to thank Air Force Research Labs (Edwards Air Force Base, CA) and Veeco Instruments (Fort Collins, CO) for funding support.

References

[1]TRIM, software available from URL: http://www.srim.org/
[2]Yalin A. P., Surla V., Farnell C., Butweiller M., and Williams J. D. 2006 Sputtering studies of multi-component materials by weight loss and cavity ring-down spectroscopy, *42nd AIAA Joint Propulsion Conference* (Sacramento, CA)
[3]Chiplonkar V. T. and Rane S. R. 1965 Dependence of angular distribution of sputtering by positive ions from metal targets on the impact angle, *Indian J. Pure Appl Phys* 3 161
[4]Tsuge H. and Esho S. 1981 Angular distribution of sputtered atoms from polycrystalline metal targets, *J. Appl. Phys.* 52 4391-95
[5]Kolasinski R. D. 2005 Oblique angle sputtering yield measurements for ion thruster grid materials, *41st AIAA Joint Propulsion Conference* 2005-3526
[6]Kolasinksi R. D., Polk J. E., Goebel D. and Johnson L. J. 2006 Carbon sputtering yield measurements at grazing incidence, *42nd AIAA/ASME/SAE/ASEE Joint Propulsion Conference* (Sacramento, CA) *AIAA* 2006-4337
[7]Zoerb K. A., Williams J. D., Williams D. D., and Yalin A. P. 2005 Differential sputtering yields of refractory metals by xenon, krypton, and argon ion bombardment at normal and oblique incidences, *29th International Electric Propulsion Conference* (Princeton, NJ) IEPC-2005-293
[8]Yalin A. P., Williams J. D., Surla V., Wolf J., and Zoerb K. A. 2006 Azimuthal differential sputter yields of molybdenum by low energy ion bombardment, *42nd AIAA/ASME/SAE/ASEE Joint Propulsion Conference* (Sacramento, CA) 2006-4336
[9]Yalin A. P., Williams J. D., Surla V., and Zoerb K. A. 2007 Differential Sputter Yield Profiles of Molybdenum due to Bombardment by Low Energy Xenon Ions at Normal and Oblique Incidence, *Journal of Physics D – Applied Physics*
[10]Mannami M., Kimura K., and Kyoshima A. 1981 Angular distribution measurements of sputtered Au atoms with quartz oscillator microbalances, *Nuclear Instruments and Methods* 185 533-37
[11]Wickersham C. E. and Zhang Z 2005 Measurement of angular emission trajectories for magnetron-sputtered tantalum, *J. Electronic Materials* 34
[12]Kundu S., Ghose D., Basu D., and Karmohapatro S. B. 1985 The angular distribution of sputtered silver atoms, *Nuclear Instruments and Methods in Physics Research B* 12 352-57
[13]Wucher A. and Reuter W. 1988 Angular distribution of sputtered particles from metals and alloys, *J. Vac. Sci. Tech. A* 6(4) 2316-18
[14]Shutthanandan V., Ray P., Shivaparan N., Smith R., Thevuthasan T., and Mantenieks M. 1997 On the measurement of low-energy sputtering yield using Rutherford backscattering spectrometry, *25th International Electric Propulsion Conference* (Cleveland, OH) IEPC-97-069
[15]Mantenieks M., Foster J., Ray P., Shutthanandan S., and Thevuthasan T. 2001 Low energy xenon ion sputtering yield measurements, *27th International Electric Propulsion Conference* (Pasadena, CA) IEPC-01-309
[16]Andersen N., B. Andresen, and E. Veje 1982 Atomic excitations in sputtering processes, *Radiation Effects* 60 119-127
[17]Doerner R.P., Whyte D.G., and Goebel D.M. 2003 Sputtering yield measurements during low energy xenon plasma bombardment, *J. App. Phys.* 93(9) 5816-5823
[18] Pellin M.J., Wright R.B., and Gruen D.M. 1981 Laser fluorescence spectroscopy of sputtered zirconium atoms, *J. Chem. Phys.* 74 6448-6457
[19] Bay H.L. 1987 Laser induced fluorescence as a technique for investigations of sputtering phenomena, *Nuclear Instruments and Methods* B18 430-445

[20]Young C.E., *et al*.1984 Velocity and electronic state distributions of sputtered Fe atoms by laser-induced fluorescence spectroscopy, *J. Vac. Sci. Technol. A* 2(2) 693-697
[21]Nicolussi G., *et al*. 1995 Formation of metastable excited Ti and Ni atoms during sputtering, *Phys. Rev. B* 51(14) 8779-8788.
[22]Goehlich A. 2001 Investigation of time-of-flight and energy distributions of atoms and molecules sputtered from oxygen-covered metal surfaces by laser techniques, *Appl. Phys. A*. 72 523-529
[23]Staudt C., et al. 2002 Sputtering of Ag atoms into metastable excited states, *Phys. Rev. B* 66 085415 1-12
[24]Surla V., Wilbur P.J., Johnson M., Williams J.D., and Yalin A.P. 2004 Sputter erosion measurements of Titanium and Molybdenum by cavity ring-down spectroscopy, *Review of Scientific Instruments* 75(9) 3025-3030
[25]Yalin A.P., Surla V., Butweiller M., and Williams J.D. 2005 Detection of Sputtered Metals using Cavity Ring-Down Spectroscopy, *Applied Optics* 44, 30 6496-6505
[26]Yalin A.P., Surla V., Farnell C., Butweiller M., and Williams J.D. 2006 Sputtering Studies of Multi-Component Materials by Weight Loss and Cavity Ring-Down Spectroscopy, *42nd AIAA Joint Propulsion Conference* (Sacramento, CA) 2006-4338
[27]Surla V. and Yalin A.P. 2007 Differential Sputter Yield Measurements using Cavity Ring-Down Spectroscopy *Applied Optics – accepted for publication*
[28]Busch K.W. and Busch M.A. 1999 *Cavity-Ringdown Spectroscopy - ACS Symposium Series 720*, ed.
[29]Berden, Peeters R., and Meijer G. 2000 Cavity Ring-Down Spectroscopy: Experimental Schemes and Applications, *Int. Reviews in Physical Chemistry* 19(4) 565-607
[30]Zalicki P. and Zare R.N. 1995 Cavity ring-down spectroscopy for quantitative absorption measurements, *Journal of Chemical Physics* 102(7) 2708-17
[31]Yalin A.P. and Zare R.N. 2002 Effect of laser lineshape on the quantitative analysis of cavity ring-down signals, *Laser Physics* 12(8) 1065-1072
[32]Jones Jr. R.E., 1972 Theories of distribution of deposit from sputtered disk and rectangular electrodes, *I.B.M. Journal of Research and Development* 27-34